Available online at www.sciencedirect.com
SCIENCE DIRECT®
ELSEVIER
International Journal of Solids and Structures 42 (2005) 5656–5668
INTERNATIONAL JOURNAL OF SOLIDS and STRUCTURES
www.elsevier.com/locate/ijsolstr

Post-yield material nonlinearity: Optimal homogeneous shear-frame sections and hysteretic behavior

T. Attard *

Department of Civil Engineering, University of New Hampshire, Durham, NH 03824-3591, United States

Received 15 October 2004
Available online 27 April 2005

Abstract

A nonlinear hardening rule that describes a general yield surface change for frame members is proposed. The rule is valid for homogeneous materials and is defined by a nonlinear constitutive model. The model is given as the stress–strain relationship through the section thickness. The post-yield behavior of shear frame members is assessed using a hardening index parameter, a plastic strain coefficient, and a smooth and optimal mathematical function to model the geometry of structural wide-flange and tube sections. This enables a continuous distribution of post-yield curvatures to exist along the member length and results in accurate finite-element member displacement predictions. Steady-state hysteresis responses are determined for frame sections using the model's nonlinearly degrading stiffness. The hardening rule is used to model the detailed material behavior of shear frame members that are subjected to lateral loads. The results of the model are validated through experimental published literature.

Keywords: Constitutive model; Degradation; Nonlinear hysteresis; Optimal sections

1. Introduction

Dafalias and Popov (1975) show that while a flow law exists when a yield surface is reached, a hardening rule is also needed to predict post-yield behavior. Such a rule can be derived as a stress–strain relationship (Shames and Cozzarelli, 1992) and be independent of rate but dependent on the history (Needleman, 1985). The resulting distribution of post-yield activity across a member's length can consequently be used to

* Tel.: +1 603 862 4447; fax: +1 603 862 2364.
E-mail address: tom.attard@unh.edu

0020-7683/$ - see front matter
doi:10.1016/j.ijsolstr.2005.03.019

accurately assess nonlinear material behavior (Bayrak and Sheikh, 2001; Kratzig and Niemann, 1996) and determine the overall energy dissipation (Popov, 1987). Oran (1973) investigates post-yield behavior by considering a small deformation/large rotation assumption to derive a tangent stiffness matrix for elastic frames. Orbison (1982) uses a finite element approach and applied shape functions to model an assumed member displacement shape and predict behavior. Kassimali and Abbasnia (1991) use a Eulerian formulation to consider large joint translations and rotations. Abbasnia and Kassimali (1995) use an idealized elastic–plastic material to model localized hinging. The modeling of ductile materials is also investigated using constitutive relationships (Marcon et al., 1999; Brunig, 1998; Barsan and Chiorean, 1999), and zero-length plastification models (Kim and Lee, 2001; Liew et al., 2000). The latter, however, do not consider the spread of plasticity along the member length (Attalla et al., 1994).

Instead, a nonlinear constitutive model and a smooth mathematical function are used to predict the spread of plasticity across wide-flange and tube cross-sections. The constitutive model is derived for homogeneous and isotropic materials as the stress–strain distribution remains the same through the section thickness. The model defines gradual plastification through the section depth and over some finite length. It is derived for uniaxial flexural deformations measured starting at the yield-state of 2D members. The model is continuous and uses a hardening index parameter (α) and a plastic strain coefficient (Δ_ε) to develop the constitutive mathematics of the stress–strain relationship. The model is an integrable stress function. Using another smooth function to optimally model the section geometry, post-yield curvature distributions along the member length can be determined. This allows lateral displacements to be accurately predicted (Bayrak and Sheikh, 2001). Although design codes (Uniform Building Code, 1997) enable practicing engineers to project nonlinear member responses using factors applied to the elastic states, the results are often conservative. Instead, the proposed model is derived at the fiber level and accurately defines post-yield behavior. The nonlinear responses are derived constitutively. A smooth function is used to model the cross-sections of frame members and smooth over the web-flange intersection. This leads to accurate finite-element member displacements and nonlinear degrading stiffness predictions.

The material model kinematically strain hardens during cyclic loading. Computer programs that model kinematic behavior (Elnashai and Izzuddin, 1993) often use a bilinear stress–strain relationship because of ease. However, a computer program that determines the nonlinear hysteresis of kinematically strain-hardened homogeneous materials has been written. The program also optimizes the parameters of a smooth function, which models the section's physical geometry. The optimization is based on minimizing the error between the actual section's internal moments and the moments of the mathematically smooth section for any post-yield state. Because the post-yield stress changes continuously, no plastic flow occurs during the hardening (Mendleson, 1968).

2. Hardening index and plastic strain coefficient

The stress and strain distributions through the section thickness are shown in Figs. 1 and 2, respectively. The post-yield stress at the top fiber of a stress state is given by $\Delta\sigma_p$; σ_y is the yield stress, and ε_y is the yield strain. The post-yield strain on the top fiber is ε_p.

The depth of linear elastic activity through the section depth is given by e. The post-yield stress and strain at some distance, y, from the neutral axis are given by σ_x and ε_x, respectively. From Fig. 2, y can be defined as $e\varepsilon_x/\varepsilon_y$. The post-yield curvature is denoted as $\Delta\phi$, and the yield curvature as ϕ_y. For the shear frame member in Fig. 3 subjected to the lateral load and moment, the depth of linear elastic activity, e, increases from a starting value at the member-end ($x = 0$) to $e = h/2$ at distance x. At $e = h/2$, the section is just-yielded, at which point x will be defined as q'. The total section depth is given as h. The post-yield states of the sections along the member length will be characterized by the linear elastic depths, e, through the section thickness.

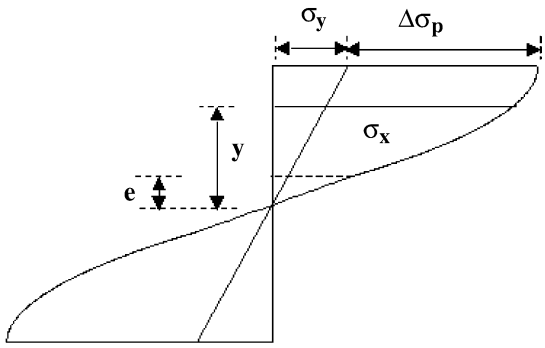

Fig. 1. Through-thickness stress distribution.

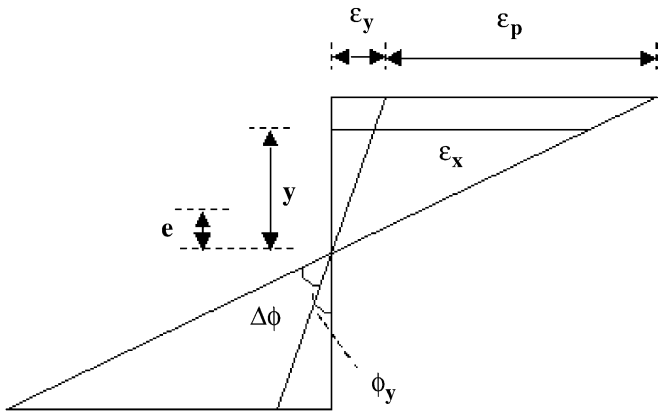

Fig. 2. Strain distribution.

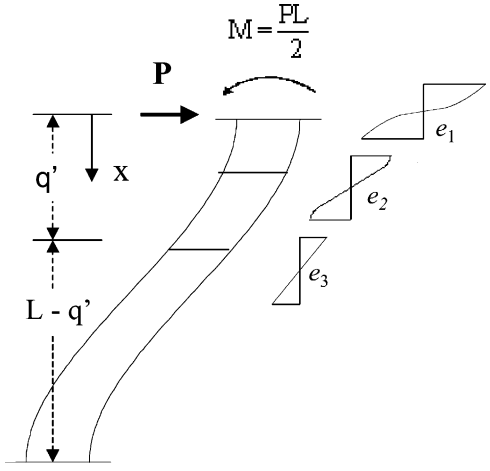

Fig. 3. Shear frame member with post-yield state distributions, e, along q'.

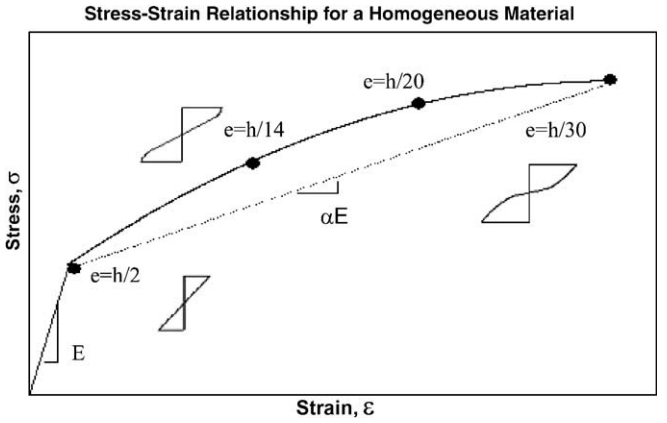

Fig. 4. Stress–strain model for a homogeneous material.

In a homogeneous material, the stress function through the section depth does not change. Fig. 4 shows the relationship for changing stress states, e, where the section's top fiber strain increases towards the ultimate strain, ε_u. The section depth, h, used is 22 in.

Eq. (1) (Attard, 2004) defines the post-yield stress at depth y for homogeneous materials as

$$\sigma_x = \sigma_y - \alpha\sigma_y\left(2 + \frac{1}{\Delta_\varepsilon}\right) + \frac{2\alpha\sigma_y y}{e}\left(1 + \frac{1}{\Delta_\varepsilon}\right) - \frac{\alpha\sigma_y y^2}{\Delta_\varepsilon e^2}. \tag{1}$$

The post-yield stress, σ_x, is a function of the plastic strain coefficient, Δ_ε, where ε_u is given by $(\Delta_\varepsilon+1)\varepsilon_y$; $\Delta_\varepsilon\varepsilon_y$ defines the plastic strain in the material when the section fails. A hardening index, α, is used to guide the stress over the post-yield activity of the material. The index defines the average modulus degradation between the yield (ε_y) and ultimate (ε_u) states and helps to create a continuous post-yield distribution. An index of 0 indicates a complete degradation of the modulus and represents an elastic–perfectly plastic case. For nonhomogeneous materials, which will be closely examined in a later investigation, a unique stress distribution would exist for each state, e. Thus, the top fiber strain would not be expressed in terms of Δ_ε since Δ_ε is a constant.

3. Geometric continuity

For nonlinear behavior, the internal moments for a post-yield state, defined by e, are found by integration (Martin, 1975; Englekirk, 1994). This enables the post-yield spread to be accurately defined. The use of discrete elements (Goldsworthy and Stevens, 1992) to compute internal beam moments results in inaccurate nonlinear lateral displacement predictions. Thus, a continuous and integrable moment function is used instead. This enables the distribution of post-yield curvatures ($\Delta\phi$) along the member length (L) to be continuous and leads to accurate lateral deflection predictions. For frame cross-sections (I-, or tube-), however, the discontinuity at the web-flange intersection region precludes a single moment function from determining the total post-yield spread distance (q') along the beam. In Eq. (2), x (also shown in Fig. 3) is the distance between the state at the end of the member (at $x = 0$) and any post-yield state along the beam, and it is given as

$$\mathrm{x} = \frac{L}{2M_E}(M_E - M_B). \tag{2}$$

The internal moments at these two states are given by M_E and M_B, respectively. For $M_B = M_y$ (where M_y is the yielded section moment), x is defined as q'. If M_E is found for state e_1 (Fig. 3) where $0 \leqslant e_1 \leqslant \frac{h}{2} - h_1$, and M_B is found for state e_3 where $\frac{h}{2} - h_1 < e_3 \leqslant \frac{h}{2}$ (h is the section depth; h_1 is the flange thickness), then a discontinuous distribution of $\Delta\phi$ along x exists because different moment functions are used in Eq. (2). Also, the summation of two spread distances (e.g., between e_1 and e_2 and between e_2 and e_3 in Fig. 3) over-estimates the true spread distance between e_1 and e_3 because of the constitutive model's nonlinearity. This over-estimation results in inaccurate stiffness and displacement predictions. This fact has been verified in a previous investigation (Attard, 2003) using a rectangular cross-section. Using the continuous function in Eq. (3), then the cross-section can be re-created as a smooth function where

$$\begin{aligned} &\text{for wide flange sections: } b = ny^c + \frac{b_1}{2}; \text{ and} \\ &\text{for tube sections: } b = ny^c + b_1. \end{aligned} \tag{3}$$

Eq. (3) correlates the moments between the actual section and a mathematical section for any post-yield state. This enables the distribution of $\Delta\phi$ along q' to be continuous. The section width at y above the neutral axis is given by b; the web thickness is b_1. The parameters n and c are used to optimally fit b to the geometry of the actual section. The sum of the residual square errors between the actual (M_a) and mathematical (M_m) section moments is minimized for any post-yield state, e_i, where $i = 1$ to n for n post-yield states. This is given in Eq. (4) for the kth iteration as

$$\begin{aligned} \text{square error}^{(k)} &= \sum_{i=1}^{n} \left(M_a(e_i) - M_m\left(e_i, n^{(k)}, c^{(k)}\right)\right)^2 \\ &\vdots \end{aligned} \tag{4}$$

The nonlinear regression terms are approximated using the Gauss–Newton method; a computer program is written to facilitate this procedure. As such, n and c are optimally found for a W30x99 section and for a 20×8 tube 1/2 in. thick. The actual and mathematical sections are shown in Fig. 5. Although n and c are associated with the web height and flange width, the two parameters have no physical relationship to the cross-section. They are only used to re-create the internal section moments for any post-yield state.

The relationship between the actual and mathematical post-yield internal moments for any state is shown in Fig. 6. The error is very small. The moment–curvature relationship in Fig. 6 is given for the W30x99 wide flange section shown in Fig. 5.

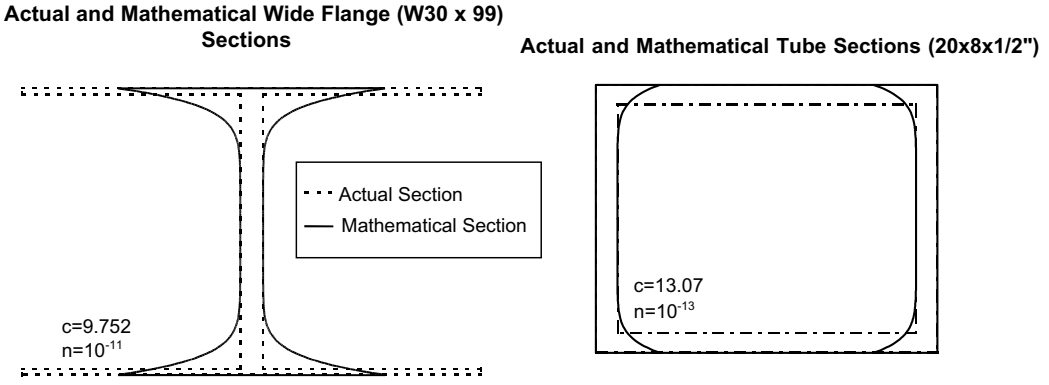

Fig. 5. Actual and mathematical sections for wide flange and tube sections.

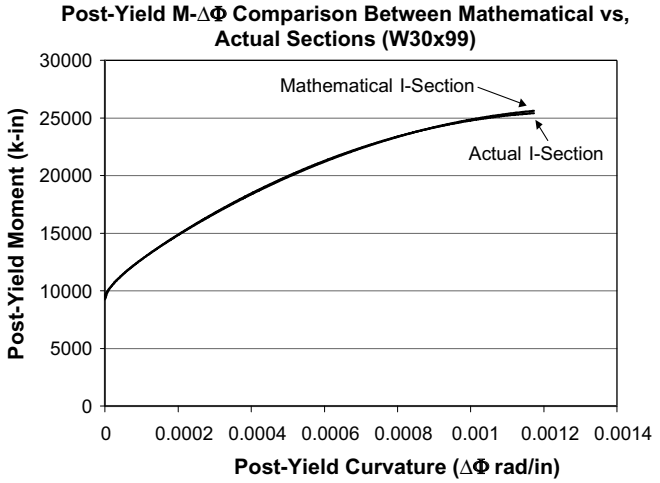

Fig. 6. Distribution of actual and mathematical internal moments.

The maximum error in the internal moments for the W30x99 section is 2.77%. A yield stress, σ_y, of 36 ksi is assumed, and the beam is loaded as in Fig. 3. The maximum error occurs at the yield state, $e = h/2$. Table 1 summarizes several I-sections, which are referenced 1–5. The maximum error between M_a and M_m is indicated for each section as is the corresponding state, e. Fig. 7 shows the distribution of the unit-less n and c parameters against the residual error for section 2 in Table 1. In general, as the ratio of h to b increases for a given b_1 and h_1 pair, the optimal c increases while n decreases. Although n and c can be adjusted to fit Eq. (3) to any cross-section, they are sensitive to perturbations. This is indicated by the fluctuations in c away from the optimum in sections 4 and 5 in Table 1. Section 3 is the optimal section with $c = 9.964$. A slight change in c results in a large increase in error.

Although the actual and mathematical sections are physically different, the purpose of applying Eq. (3) is to predict nearly identical state moments between the two sections. The continuous geometry enables a continuous curvature distribution to exist along the member length.

4. Analysis of post-yield terms

Using σ_x in Eq. (1), the internal moments for the actual frame cross-section are given in Eqs. (5) and (5a) as

Table 1
Five I-sections fitted to Eq. (3)

Section no.	I-Section dimensions (in.)				Parameters		Max moment state	
	b	h	b_1	h_1	n	c	%Error	e (h)
(1)	10	22	2	3	1×10^{-8}	8.634	1.93	0.5
(2)	10	36	2	3	8×10^{-11}	8.695	0.549	0.439
(3)	10	48	2	3	1×10^{-13}	9.964	0.595	0.463
(4)	10	48	2	3	1×10^{-13}	9.900	10.72	0.472
(5)	10	48	2	3	1×10^{-13}	10.00	6.551	0.371

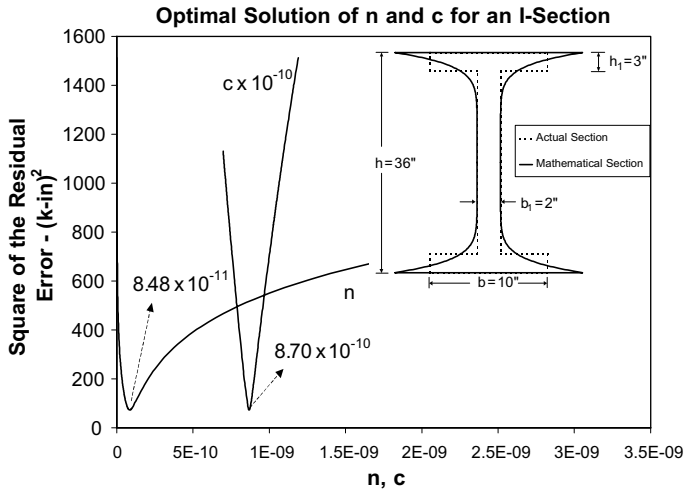

Fig. 7. Optimal relationship of n and c for section 2 in Table 1.

$$M=\sigma_y\left\{(b_1-b)\left(\frac{h}{2}-h_1\right)^2\left[1-\alpha\left(2+\frac{1}{\Delta_\varepsilon}\right)+\frac{4\alpha}{3e}\left(\frac{h}{2}-h_1\right)\left(1+\frac{1}{\Delta_\varepsilon}\right)-\frac{\alpha}{2\Delta_\varepsilon e^2}\left(\frac{h}{2}-h_1\right)^2\right]\right.$$
$$\left.-b_1e^2\left[1-\alpha\left(2+\frac{1}{\Delta_\varepsilon}\right)+\frac{4\alpha}{3}\left(1+\frac{1}{\Delta_\varepsilon}\right)-\frac{\alpha}{2\Delta_\varepsilon}-\frac{2}{3}\right]+\frac{bh^2}{4}\left[1-\alpha\left(2+\frac{1}{\Delta_\varepsilon}\right)+\frac{2\alpha h}{3e}\left(1+\frac{1}{\Delta_\varepsilon}\right)-\frac{\alpha h^2}{8\Delta_\varepsilon e^2}\right]\right\}$$
$$\ldots 0<e\leqslant\left(\frac{h}{2}-h_1\right), \tag{5}$$

$$M=2\sigma_y\left\{\frac{(b_1-b)}{3e}\left(\frac{h}{2}-h_1\right)^3+b\left[\frac{(h^2-4e^2)}{8}-\frac{\alpha(h^2-4e^2)}{8}\left(2+\frac{1}{\Delta_\varepsilon}\right)+\frac{\alpha}{12}\left(\frac{h^3}{e}-8e^2\right)\left(1+\frac{1}{\Delta_\varepsilon}\right)\right.\right.$$
$$\left.\left.-\frac{\alpha}{64\Delta_\varepsilon}\left(\frac{h^4}{e^2}-16e^2\right)+\frac{e^2}{3}\right]\right\}\ldots\left(\frac{h}{2}-h_1\right)\leqslant e<\frac{h}{2}. \tag{5a}$$

For a state $e<(h/2–h_1)$, the beam's lateral displacements cannot be accurately determined. This is because of the discontinuity at the web-flange intersection of frame sections. Using Eqs. (1) and (3), the entire range of post-yield activity along a member's length can be determined. This is accomplished by applying a single continuous moment function, which is conducive to a geometrically continuous section, into Eq. (2). This moment function is given in Eq. (6) as

$$M=4\sigma_y\left\{n\frac{h^{c+2}-2^{c+2}e^{c+2}}{2^{c+2}(c+2)}+b_1\frac{h^2-4e^2}{8}-\left(2+\frac{1}{\Delta_\varepsilon}\right)\left[n\alpha\frac{h^{c+2}-2^{c+2}e^{c+2}}{2^{c+2}(c+2)}+b_1\alpha\frac{h^2-4e^2}{8}\right]\right.$$
$$+\left(1+\frac{1}{\Delta_\varepsilon}\right)\left[2\alpha n\frac{h^{c+3}-2^{c+3}e^{c+3}}{2^{c+3}(c+3)e}+b_1\alpha\frac{h^3-8e^3}{12e}\right]-\frac{1}{\Delta_\varepsilon e^2}\left[\alpha n\frac{h^{c+4}-2^{c+4}e^{c+4}}{2^{c+4}(c+4)}+b_1\alpha\frac{h^4-16e^4}{64}\right]$$
$$\left.+\frac{n}{c+3}e^{c+2}+\frac{b_1}{3}e^2\right\}. \tag{6}$$

5. Post-yield spread

Eq. (6) is used to derive a nonlinear distribution of curvatures. The total post-yield spread, q', along the beam is defined by Eq. (2) when $M_B = M_y$ at the yield state $e = h/2$. Defining M_E by Eq. (6), q' is calculated for frame members and becomes plotted as a function of $\Delta\phi$. When full plastification at $x = 0$ occurs, M_E becomes the ultimate moment (M_u), and q' is the plastic hinge length, L_p.

The post-yield curvature at the end of the member ($\Delta\phi$ at $x = 0$) increases as q' increases. However, as $\Delta\phi$ approaches the plastic curvature (ϕ_p), the rate at which q' increases tends to decrease. Thus, most of the post-yield spread along the beam occurs during the early stages of post-yield activity. This is indicated in Fig. 8 by the relationship between q' and $\Delta\phi$ at $x = 0$. Two different values of α are used. The optimal c and n parameters are determined. In general, an increase in α results in an increase in c and a decrease in n. The plastic strain coefficient, Δ_ε, is assumed to be 14. The distributions are shown along a half-beam length ($L/2$) for a tube section $18 \times 12 \times 1/2$ in.; $L = 120$ in.; $\sigma_y = 36$ ksi. Although q' increases minimally as the section tends towards full plastification, the area of post-yield activity under the $\Delta\phi$ (at $x = 0$) vs. q' relationship increases steadily. The units under $\Delta\phi - q'$ are in./in. Fig. 9a ($\alpha = 0.25$) and 9b ($\alpha = 0.1$) show the distribution $\Delta\phi$ along the beam for different strains at $x = 0$. On the horizontal axis, the distance, x (Eq. 3), away from the member end is shown. For example, when the curve for $\varepsilon = 4\varepsilon_y$ reaches the horizontal axis, x becomes q'. Assuming $\Delta_\varepsilon = 14$, full plastification (ε_u) is reached when $\varepsilon = 15\varepsilon_y$. Thus, when the $\varepsilon = 15\varepsilon_y$ curve reaches the horizontal axis, $x = q'$ is defined as L_p. The concentration of the area under the $\Delta\phi - q'$ graph increases as the member-end strains (Figs. 9a and b) increase. The concentration is measured from the end of the member at $x = 0$. However, the rate of this increase is less than the rate of increase in the area. Thus, the ratio of concentration distance to area decreases as the strains at the end of the member increase. This indicates that larger member-end strains have a greater impact on the lateral deflection predictions than smaller strains. While changing α impacts the concentration and area, it does not affect their ratio. This is shown in Table 2 for a W18x50 section. The results are normalized to $\alpha = 0.25$ ($\Delta_\varepsilon = 14$). For $\alpha = 0.15$, the post-yield concentration location and area are both 87% of those for $\alpha = 0.25$. Thus, while the member deflections decrease as α decreases, the deflection predictions are mostly impacted at roughly the same latter stages of plastification. For $\Delta_\varepsilon = 14$, this impact has been shown to begin at around $\varepsilon = 11\varepsilon_y$.

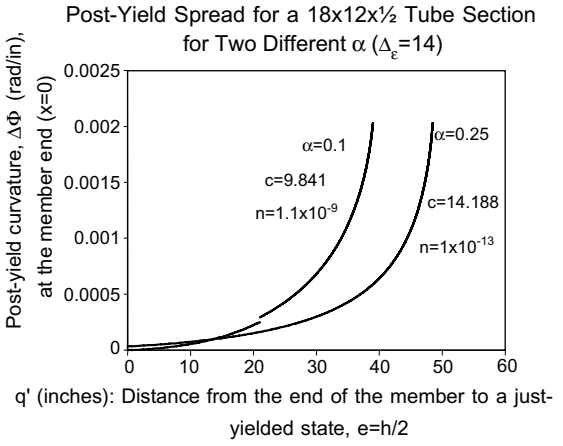

Fig. 8. Member-end $\Delta\phi$ distribution for q'.

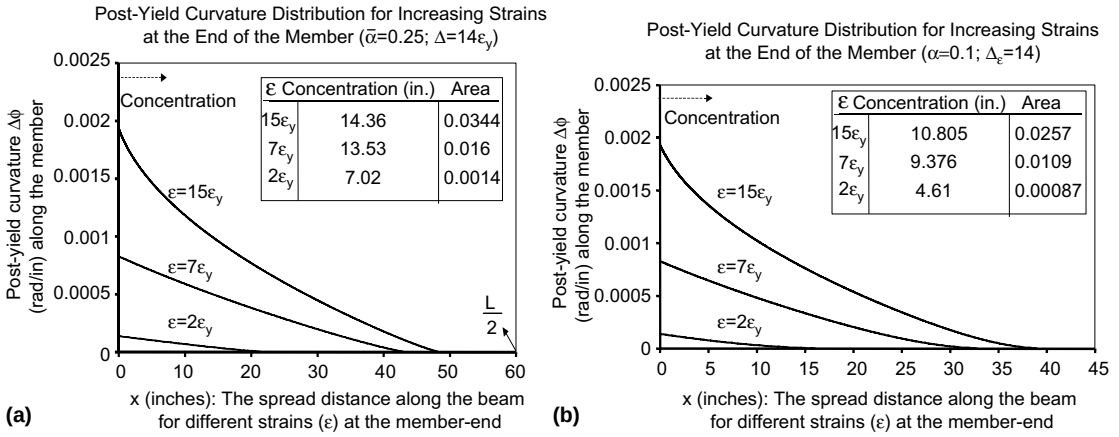

Fig. 9. (a) $\Delta\phi$ distribution along x for varying strains at $x = 0$. $\alpha = 0.25$ and (b) $\Delta\phi$ distribution along x for varying strains at $x = 0$. $\alpha = 0.1$.

Table 2
Impact of α on the post-yield activity (W18x50)

α	Concentration location and area as a percentage—normalized to $\alpha = 0.25$		
	Concentration	Area	Ratio
0.25	100%	100%	1
0.15	87%	87%	1
0.1	75%	75%	1
0.05	54%	53%	1.02
0.01	19%	18%	1.06

Deflections are determined by integrating q' with respect to $\Delta\phi$. Eq. (7) defines the member-end plastic deflection (Δ_p) where $q' \equiv f(\Delta\phi)$, and ϕ_p is the plastic curvature (Attard, 2004).

$$\Delta_p = L\int_0^{\phi_p} f(\Delta\phi)\,d(\Delta\phi) - \frac{1}{2}\int_0^{\phi_p} f^2(\Delta\phi)\,d(\Delta\phi). \tag{7}$$

6. Hysteretic responses

A computer program code, written in Visual Basic, is used to define the material hysteresis for various frame members, as in Fig. 3. The material is assumed to kinematically strain harden, however, the elastic stiffness remains unchanged during unloading and reloading. Ultimately, the model can be used to predict the steady-state displacements of members that are part of a multi-story shear frame building. In a dynamic environment, the model is applicable once the transient component of the response vanishes. Hysteretic responses are shown in Figs. 10a–d. Quasi-static loads are used to simulate the steady-state behavior of a W18x50 section ($c = 10.807$; $n = 1.4 \times 10^{-10}$) and also the I-beam listed in Table 1 as section 2 ($c = 8.695$; $n = 8.48 \times 10^{-11}$). σ_y is assumed to be 36 ksi, and the member length is 120 in. Figs. 10a and b show the two sections responding at larger member-end strains ($13.31\varepsilon_y$ and $11.67\varepsilon_y$, respectively) as they tend towards full section plastification. The member in Fig. 10c responds at a lower member-end strain.

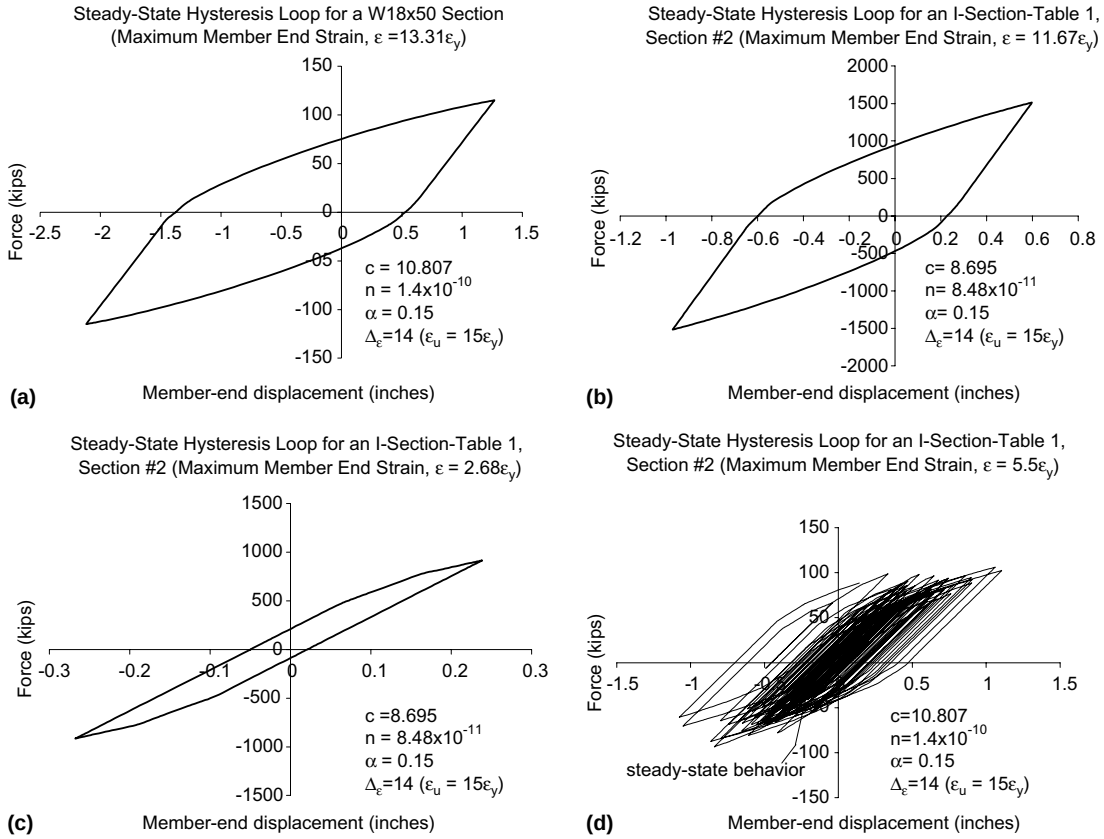

Fig. 10. (a) W18x50—quasi-static load; (b) and (c) I-section Table 1—quasi-static load; (d) W18x50—white noise loading.

Finally, the W18x50 section with little mass is excited with white noise input. The hysteretic response is shown in Fig. 10d. The member response is shown to be mostly steady-state for which the model is applicable. The member-end strains range roughly between $4\varepsilon_y$ and $5.5\varepsilon_y$. An index of 0.15 and $\Delta_\varepsilon = 14$ is used in all cases.

Table 3 shows the average stiffness between the just-yielded state and the ultimate state. It also shows the remaining stiffness at various strain states at the member-end. The stiffness that remains is given as a percent of the original nondegraded stiffness. Instead of defining gradual member degradation, the Uniform Building Code (1997) uses 25% of the original stiffness to denote the abrupt formation of a plastic hinge. Thus, sections other than the hinged section remain linearly elastic; the ultimate deflection is determined using the plastic moment defined from a perfectly plastic stress–strain relationship. While this does not result in accurate displacement predictions, the 25% degradation value can be used to help select α and Δ_ε. For the W18x50 section, $\alpha = 0.15$ is a reasonable selection since the overall average degradation is 26% and the 25% code value is captured at around the mid-level post-yield strain of $6\varepsilon_y$ (where $\varepsilon_u = 15\varepsilon_y$). For the I-beam in Table 1 (section 2), 25% of the original stiffness remains when the post-yield strain reaches $7.5\varepsilon_y$, which is a mid-amount of straining between the first and ultimate states ($\varepsilon_u = 15\varepsilon_y$). Also, the average stiffness is 28%, which is close to 25%. Using these criteria, the use of $\alpha = 0.15$ and $\Delta_\varepsilon = 14$ seems reasonable.

Table 3
Discretized stiffnesses as a percentage of the nondegraded stiffness

Strain range	Stiffness percentages				
	α				
	0.25	0.15	0.2	0.1	0.05
$\varepsilon_y - 2\varepsilon_y$	74	64	69	59	55
$3\varepsilon_y - 4\varepsilon_y$	49	34	42	27	21
$5\varepsilon_y - 6\varepsilon_y$	42	28	35	21	14
$6\varepsilon_y - 7\varepsilon_y$	39	25	32	19	13
$7\varepsilon_y - 8\varepsilon_y$	37	23	30	17	11
$10\varepsilon_y - 11\varepsilon_y$	29	18	24	13	8
$14\varepsilon_y - 15\varepsilon_y$	17	11	14	8	5
Average %	40	26	33	21	15

Degradation from $\varepsilon_y - 15\varepsilon_y$ ($\Delta_\varepsilon = 14$).

Table 4
Discretized displacements along W18x50 section. $\alpha = 0.1$

Strain at x	x (in.)	Displacement (in.)
ε_y	$37.9 = L_p$	2.16
$2\varepsilon_y$	31.0	2.37
$4\varepsilon_y$	22.9	2.59
$7\varepsilon_y$	13.2	2.81
$9\varepsilon_y$	8.2	2.89
$11\varepsilon_y$	4.4	2.93
$14\varepsilon_y$	0.7	2.94
$15\varepsilon_y$	0.0	2.95

7. Finite element displacements

The finite element displacements of the member over the plastic hinge length are shown in Table 4 ($\alpha = 0.1$; $\Delta_\varepsilon = 14$) for a W18x50 section ($L_p = 37.9$ in.). The section is discretized into elements bounded by increasing strain levels. A distribution of the member displacements is shown in Fig. 11 for W18x50 ($c = 10.807$; $n = 1.4 \times 10^{-10}$) and W30x99 ($c = 9.752$; $n = 1 \times 10^{-11}$) sections ($L = 120$ in., $\sigma_y = 36$ ksi). Because the material is nonlinear, the tip displacement (at $x = 0$) at yield (0.20 in.) does not equal the displacement (1.32 in.) of the yielded section located at L_p.

8. Test verification with a cantilever beam

The nonlinear hardening model is verified with a cantilevered test specimen (Englekirk, 1994). The results are favorable. The specimen is a W18x50 steel section ($\sigma_y = 24$ ksi; $L = 83.11$ in.) subjected to a quasi-static load. Selecting α to be 0.15 and $\Delta_\varepsilon = 14$ predicts an average stiffness over the post-yield activity of 26% of the nondegraded stiffness. Furthermore, at a mid-level strain of $7\varepsilon_y$, the remaining stiffness is 25% of the original stiffness. Thus, $\alpha = 0.15$ and $\Delta_\varepsilon = 14$ will be used. The optimum value of c is 12.881; the optimum value for n is 1.7×10^{-12}. The displacement ductility is determined as 9.76 using the model while the test shows the ductility to be near 11. Also, the first yield deflection (0.21 in.) agrees with the test result at the end load of 25 k. At a load 38 k, the actual deflection is 0.45 in.; the model predicts 0.40 in. The

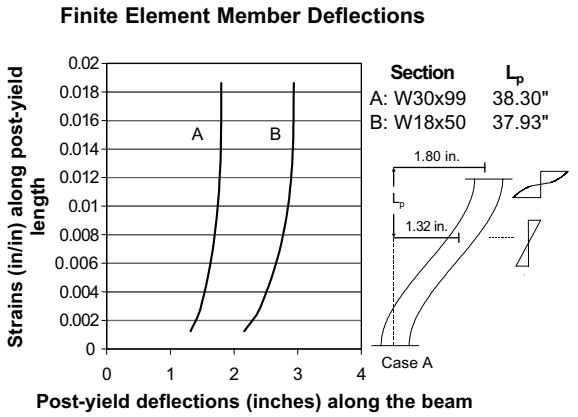

Fig. 11. Finite element displacement distributions.

displacement predicted at a load of 44 kips is 0.54 in. while the test indicates that the displacement should be 0.6 in. At this point in the test, the published literature creates a linear post-yield curvature distribution. Working back from the 0.6 in. deflection, the post-yield spread (q') is determined as 34.3 in. The model predicts q' to be 35.6 in. These spread distances are similar even though the literature linearizes the post-yield curvature distribution. The literature also uses the linear $\Delta\phi$ distribution to predict a strain at the member-end ($x = 0$) of $2.5\varepsilon_y$. Since the model is nonlinear, a larger strain of $3.3\varepsilon_y$ is predicted. Nearing the ultimate state on the specimen, a load of 68 kips produces a displacement of 2.3 in. The model, however, predicts a displacement of 2.3 in. at a load of 80 kips. This difference could be attributed to the test specimen's hysteresis, which reduces the elastic stiffness during re-loading. The model does not account for this. Very little energy had been dissipated in the test specimen at the time of the other measured load–displacement points discussed.

9. Conclusions

A nonlinear material hardening model is proposed for frame members. The model enables post-yield responses to be more accurately predicted. The model is valid for in-plane flexural deformations where axial and shear deformations are neglected. The model defines material behavior through a hardening index, α, which outlines the level of post-yield degradation through the constitutive relationship. A plastic strain coefficient, Δ_ε, is used to project the ultimate state. Using a continuous mathematical cross-section, internal post-yield moments can be determined using a single function. Parameters of the continuous section are optimally determined. This is successfully accomplished by minimizing the error between the internal moments of the actual section and those of the physically continuous section. Since α and Δ_ε are used in both sections, they cannot be optimally determined. Instead, they can be determined using code guidelines. Doing so has been shown to result in accurate response predictions. Nonetheless, future testing will provide more physical test data that can be used to optimally determine α and Δ_ε as well.

Deriving a single (optimal) moment function for any post-yield state of the frame member enables a continuous curvature distribution to exist along the member. This allows finite-element member deflections and the plastic hinge length to be accurately predicted. Furthermore, the model can also be used to model the steady-state hysteretic response of shear frame members although elastic stiffness loss is neglected during reloading of the member. The results of the model are verified against a cantilevered beam test. The results compare favorably.

References

Abbasnia, R., Kassimali, A., 1995. Large deformation elastic–plastic analysis of space frames. Journal of Constructional Steel Research 35 (3), 275–290.

Attalla, M., Deierlein, G., McGuire, W., 1994. Spread of plasticity: quasi-plastic-hinge approach. Journal of Structural Engineering 120 (8), 2451–2473.

Attard, T., 2003. Modeling of higher-mode effects in various frame structures using a pushover analysis. In: Doctoral Dissertation. Arizona State University, Tempe, Arizona.

Attard, T., 2004. Post-yield material analysis and plastic hinge assessment of frame members. In: Proceedings of the Eighth Pan American Congress of Applied Mechanics. Havana, Cuba, ISBN 959-7056-20-8, pp. 503–507.

Barsan, G., Chiorean, C., 1999. Computer program for large deflection elasto-plastic analysis of semi-rigid steel frameworks. Computers and Structures 72 (6), 699–711.

Bayrak, O., Sheikh, S., 2001. Plastic hinge analysis. Journal of Structural Engineering 127 (9), 1092–1100.

Brunig, M., 1998. Nonlinear finite element analysis based on a large strain deformation theory of plasticity. Computers and Structures 69 (1), 117–128.

Dafalias, Y., Popov, E., 1975. A model of nonlinearly hardening materials for complex loading. Acta Mechanica 21 (3), 173–192.

Elnashai, A., Izzuddin, B., 1993. Modeling of material nonlinearities in steel structures subjected to transient dynamic loading. Earthquake Engineering and Structural Dynamics 22 (6), 509–532.

Englekirk, R., 1994. Steel Structures: Controlling Behavior through Design. John Wiley & Sons, New York.

Goldsworthy, H., Stevens, L., 1992. Energy dissipation in determinate steel beams. Journal of Structural Engineering 118 (1), 1–17.

Kassimali, A., Abbasnia, R., 1991. Large deformation analysis of elastic space frames. Journal of Structural Engineering 117 (7), 2069–2087.

Kim, S., Lee, J., 2001. Improved refined plastic-hinge analysis accounting for local buckling. Engineering Structures 23 (8), 1031–1042.

Kratzig, W., Niemann, H., 1996. Dynamics of Civil Engineering Structures. A.A. Balkema, Netherlands.

Liew, J., Chen, H., Shanmugam, N., Chen, W., 2000. Improved nonlinear plastic hinge analysis of space frame structures. Engineering Structures 22 (10), 1324–1338.

Marcon, A., Bittencourt, E., Creus, G., 1999. On the integration of stresses in large deformations plasticity. Engineering Computations 16 (1), 49–69.

Martin, J., 1975. Plasticity: Fundamentals and General Results. MIT Press, Massachusetts.

Mendleson, A., 1968. Plasticity: Theory and Application. Macmillan Publication, New York.

Needleman, A., 1985. On finite element formulations for large elastic–plastic deformations. Computers and Structures 20 (1-3), 247–257.

Oran, C., 1973. Tangent stiffness in space frames. ASCE Journal of Structural Divisions 99 (ST6), 987–1001.

Orbison, J., 1982. Nonlinear static analysis of three-dimensional steel frames. In: Report No. 82-6. Cornell University, Ithaca, New York.

Popov, E., 1987. Panel zone flexibility in seismic moment joints. Journal of Constructional Steel Research 8, 91–118.

Shames, I., Cozzarelli, F., 1992. Elastic and Inelastic Stress Analysis. Prentice Hall, New Jersey.

Uniform Building Code, 1997. International Conference of Building Officials. Pasadena, Calif.